Int. J. Multiphase Flow Vol. 16, No. 6, pp. 1003–1021, 1990
Printed in Great Britain.

0301-9322/90 $3.00 + 0.00

DEEP SWIRLING FLOW DOWN A PLUGHOLE WITH AIR ENTRAINMENT

G. C. GARDNER
National Power Technology and Environmental Centre, Kelvin Ave, Leatherhead, Surrey, England

(*Received* 29 *November* 1989; *in revised form* 12 *July* 1990)

Abstract—Experiments have been carried out to determine the water depth required to entrain a given amount of air with a given circulating water flow discharging through a vertical pipe set in the flat bottom of a vessel. The circulation angle, α, between the radial direction and the velocity vector far from discharge pipe was set at 0°, 10°, 30° or 60°.

It is shown that results are not dependent upon the diameter of the offtake pipe, if that is sufficiently small, and results are then expressed either as a dimensionless water depth vs a dimensionless ratio of the flow rates of the two phases or as a dimensionless flow rate of one phase vs the dimensionless flow rate of the other phase. An approximate theory describes trends in the data and is mostly in good quantitative agreement.

The results are used to examine the work of others on the entrainment of air or steam by water flowing along the bottom of a horizontal pipe into a small bottom offtake and the similar entrainment of water by air or steam flowing into a small top offtake. These systems occur in certain PWR loss of coolant accidents.

Key Words: air entrainment, swirling flow, plughole, PWR LOCA

1. INTRODUCTION

Most of us, at least as children, have been fascinated by the vortex which occurs when a bathtub is emptied, especially when sound effects accompany the entrainment of air. It is, therefore, surprising that the subject has received relatively little scientific attention. One source of technical interest is the prevention of entrainment of the supernatant phase, which may be gas, vapour or a less dense miscible or immiscible liquid. Studies of critical entrainment conditions have been made by, amongst others, Davidian & Glover (1956), Harleman *et al.* (1959), Lubin & Springer (1967), Gardner & Crow (1971), Jain *et al.* (1978) and Munson (1988), for cases in which there is no circulation, and by Springer & Patterson (1969), Smoglie & Reimann (1986), Schrock *et al.* (1986) and Gulliver & Rindels (1987), where there is at least circulation in the lower phase, though for the last three the circulation was of unknown magnitude.

Another source of interest concerns a device used in water or sewage works called a vortex drop. Here fluid is introduced tangentially into a large open tank and is discharged through a pipe set centrally in the tank's bottom. As expected, the fluid adheres to the pipe's walls as a rotating mass surrounding an air core. Binnie & Teare (1956) developed the theory of the vortex drop to give a discharge rate in terms of the fluid depth in the tank and the circulation strength. They and, later, Jain (1987) carried out experimental work.

The theory of Binnie & Teare (1956) is closely related to that for the discharge of water from a lake over a broad-crested weir or into a horizontal pipe which does not run full. In the last case, an energy balance is written for the water which relates the discharge rate to the difference in level between the water on the weir and in the lake. The level difference that maximizes the discharge rate is chosen and, then, the water velocity on the weir is that which just prevents a small interfacial disturbance moving upstream. In the case of the vortex drop, an energy balance is also drawn up and the flow is maximized with centrifugal acceleration partly replacing that due to gravity.

Gardner (1988) studied the flow of both air and water from a stratified condition in a large vessel into a horizontal pipe and showed that, for sufficiently small discharge rates, the flow rate of one phase could be maximized, with the flow rate of the other phase held constant, to predict the interface level in the large vessel in agreement with experiment. However, it was shown theoretically that, when the flow rates become sufficiently large, the position, which is called the control point, at which a small interfacial disturbance is just prevented from moving upstream passes out of the

entrance of the pipe back into the vessel. Discharge rates with respect to the level in the vessel then become independent of the diameter of the pipe. Indeed, stratified conditions are only needed up to the control point and can break down thereafter. The theory gave good quantitative agreement with the experiments and also agreed with results obtained by Smoglie & Reimann (1986), Schrock *et al.* (1986) and Anderson & Benedetti (1986) for a wide range of conditions using both air–water and steam–water systems. Moreover, all these sets of authors used small offtake pipes such that the flow was broken down to a homogeneous condition within the pipe.

The present work is an experimental and theoretical study of the flow of air and water together out of a pipe set in the bottom of a vessel, with known circulation imposed upon the water. The diameter of the pipe employed is sufficiently small for it not to be a parameter influencing the interface level required in the vessel to effect discharge. If the offtake diameter is large, it is to be assumed that the theory of Binnie & Teare (1956) for water flow alone may be modified for the flow of two phases in a similar manner to the modification carried out by Gardner (1988) with respect to a horizontal pipe.

The impetus for the work derives from PWR small loss-of-coolant accident (LOCA) studies where the rate of discharge of steam and water is important in determining the course of the accident. Schrock *et al.* (1986) and Smoglie & Reimann (1986) had the same reason for their work but, although the latter noted the strong influence of the circulation of the water, they could not measure its strength. The results to be reported here will demonstrate quantitatively the role played by circulation.

2. THE APPARATUS

The apparatus is illustrated in figure 1. The test vessel was a stainless steel cylinder 380 mm tall with i.d. = 345 mm. It was enclosed by stainless steel end plates. Water was supplied from a recirculating system and was metered by rotameters. It was fed into the bottom of the test vessel

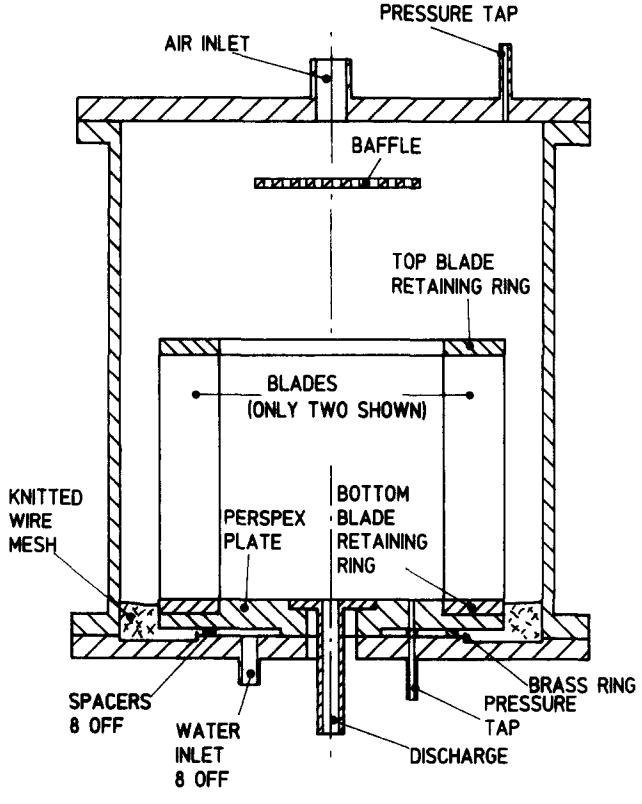

Figure 1. Cross-section through the apparatus.

through eight 12.7-mm bore tubes on a pitch circle diameter of 130 mm. A Perspex plate with a diameter of 280 mm was set 6 mm above the bottom of the vessel on a central 80 mm diameter stand and upon eight 10-mm diameter spacers on a 200 mm pitch circle diameter. Water and air together were discharged through a central vertical pipe with its top set flush with the top of the Perspex plate. The bore of the discharge was 14.51 mm for most of the work but a 26.31 mm bore pipe was also used. The discharge pipe was connected to a flexible hose which ran 2 m downwards to beneath the water level in the water's recirculation tank, in which the air was separated. A by-pass in the flexible hose passed through a pump, which was sometimes used to assist the flow.

Water flowing into the bottom of the test vessel flowed in the 6 mm gap beneath the Perspex plate to a brass ring of 217 mm diameter which provided a circumferential orifice 4 mm deep. Beyond the ring the stainless steel bottom plate was milled out to increase the gap between the Perspex plate and the bottom plate to 10 mm.

Ninety aluminium blades, 51 mm wide and 200 mm tall were made with the cross-section shown in figure 2. They were set vertically and equally spaced on the top of the Perspex plate with their thick ends at the edge of the plate at a diameter of 280 mm. The blades were accurately positioned top and bottom by setting them in Perspex rings with milled slots. The lower ring was set in a milled recess in the Perspex plate so that there was no step for the water to flow over in passing through the blades. Pairs of rings were milled to set the blades in four positions at 0°, 10°, 30° and 60° to the radial.

Air was metered by rotameters whose direct reading was l/min of air at 1 bar and 20°C. It flowed into the centre of the top of the vessel through a 22 mm bore pipe and impinged upon a 130 mm diameter baffle set 45 mm below the top plate of the test vessel. The baffle contained 32 5.5-mm diameter holes. The rotameters operated at the test vessel pressure, which was measured from a tapping in the top plate by a mercury manometer at up to 2.2 bar and by a Bourdon gauge for higher pressures up to 3.2 bar.

The water level in the test vessel with respect to the top of the Perspex plate was measured by a manometer connected to a tapping flush with the Perspex plate at a radial position 65 mm from the axis of symmetry and to a tapping in the top plate of the test vessel.

The apparatus described above did not allow visual examination of the flow but the first form of apparatus used a Perspex instead of a stainless steel test vessel. A change was only made when it was concluded that pressures up to 3 bar would be needed to study the complete parameter range. The early work showed that, although the design was meant to provide a uniform flow of water up the height of the blades, the water entering the annulus between the blades and the vessel wall was disturbed and the uniformity of flow was in doubt. Therefore, a ring of knitted wire mesh was inserted in the annulus up to the level of the top of the Perspex plate, as shown in figure 1, and this calmed the flow. Prior to this modification, results were obtained which appeared to be influenced by a parameter not included in the theory, which is described later. Insertion of the mesh removed the variation. In general, it may be noted that the successful correlation of the results by dimensionless groups arising out of the theory supports the conclusion that the required ideal air and water flow system was obtained during the experiments.

The method of operation was usually to set a water flow rate and then to raise the air flow rate in steps. The water level in the test vessel adjusted rapidly for each change of air flow rate and

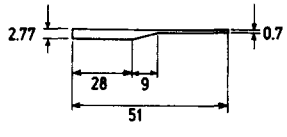

Figure 2. Cross-section through a blade.

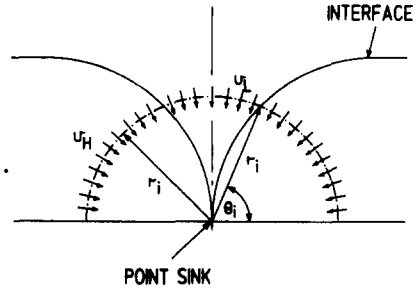

Figure 3. Assumed radial flow system.

was measured together with the test vessel pressure. However, results did not depend upon whether it was the water or air flow rate that was varied or on whether the flow rates were being raised or lowered.

3. VISUAL OBSERVATIONS

With the blades set radially, the interface between the water and the air, including the trumpet-shaped part leading down to the outlet, was smooth. Bubbles introduced at the interface through a hypodermic showed that the flow was radial. Also, the trumpet was accurately centred on the axis of the outlet. The same observations were made with the blades set at 10° to the radial, except that bubbles at the interface showed circulation to be occurring.

With blades set at 30° to the radial and with lower air flow rates, the interface, including the top part of the trumpet, was smooth. Lower down the trumpet became ragged and appeared to increase in diameter before it entered the offtake, though it should be noted that, with the blades set at more than 10° to the radial, the system could only be viewed downwards through the top of the Perspex vessel. At higher air flow rates, the axis of the vortex rotated in the direction of circulation with a frequency of about 1 Hz and the vortex appeared to attach itself to the wall of the outlet. Spiral capillary waves were present at the interface and, at the same time, a wave with the same frequency circulated in the annulus between the blades and the test vessel wall. The measured water level oscillated, though, usually, only by $< \pm 0.5$ mm, even with the larger bore outlet. At higher air flow rates still, the circulation of the vortex stopped.

With blades at 60° to the radial, the visual observations at low and intermediate air flow rates were similar to those with blades at 30° to the radial, though the circulation of the vortex appeared less strong. Perhaps this was because the depth of flow was greater, it being noted that flow depth increases as the circulation increases. However, when the direct rotameter reading reached about 200 l/min at 1 bar and 20°C as opposed to the maximum attainable value of 600 l/min, a new phenomenon set in. The measured water level oscillated slowly and erratically over a substantial range. This caused the air pressure and flow rate also to oscillate. It was clear that the apparatus would need to be redesigned if this phenomenon were to be examined and such results are excluded from this study. However, the occurrence of the phenomenon emphasizes that, although the results to be presented may be interpolated, they should not be extrapolated.

Lastly, it is noted that with blades set at 30° to the radial, with the larger 26.31 mm outlet and with a high water flow rate of 2.45 kg/s, slow irregular oscillations of the water level also occurred at a direct rotameter reading of 45 l/min. They did not occur with a water flow rate of 2.2 kg/s.

4. THEORY

Analysis of flows with a free surface of the kind of interest here are notoriously difficult and exact solutions may only be obtained numerically with a computer. Therefore, an approximate analysis is presented, which can be judged against the experimental results to see if it contains the essential mechanisms of importance.

Figure 3 illustrates the assumed flow system. Polar coordinates (r, θ) are used and the interface has coordinates (r_i, θ_i). With respect to any particular point on the interface, each phase is assumed to flow as if to a uniform point sink with a velocity v_H for the heavy or water phase and a velocity v_L for the light or air phase. Subscripts H and L will denote heavy and light phases throughout. In addition, the water phase is assumed to circulated about the axis of symmetry with a velocity v_c such that $v_c R$ is constant. R is the radial distance from the axis of symmetry and equals $r \cos \theta$. These statements are in accord with simple potential flows but the assumed direction of flow at the interface is not parallel to the interface, as it should be. However, those, such as Harleman *et al.* (1959) and Lubin & Springer (1967), studying the conditions for the inception of entrainment without circulation have used the assumption of uniform radial flow with some success. It will be seen that the assumptions are probably more justified in the present more general case.

Let Q be a constant volumetric flow rate. The assumptions can be stated as

$$Q_H = 2\pi r_i^2 v_H \sin\theta_i, \quad [1]$$

$$Q_L = 2\pi r_i^2 v_L (1 - \sin\theta_i) \quad [2]$$

and

$$v_c r_i \cos\theta_i = C, \quad [3]$$

where C is a constant.

Let the subscript ∞ denote conditions as $R \to \infty$. Then

$$v_{c\infty} = \frac{C}{R_\infty} = v_{H\infty} \tan\alpha \quad [4]$$

and

$$Q_H = 2\pi R_\infty h_\infty v_{H\infty}, \quad [5]$$

where h is the height of the interface above the bottom and α is called the circulation angle, which is the angle between the radial direction and the velocity vector or the blade angle to the radial.

The constant C is obtained by eliminating $v_{H\infty} R_\infty$ between [4] and [5] and then, from [3],

$$v_c = \frac{Q_H \tan\alpha}{2\pi r_i h_\infty \cos\theta_i}. \quad [6]$$

Next, energy balances are written for each phase between an arbitrary position on the surface and at the interface at $R = \infty$:

$$p + \frac{\rho_H v_H^2}{2} + \frac{\rho_H v_c^2}{2} + \rho_H g r_i \sin\theta_i = p_\infty + \rho_H g h_\infty \quad [7]$$

and

$$p + \frac{\rho_L v_L^2}{2} + \rho_L g r_i \sin\theta_i = p_\infty + \rho_L g h_\infty, \quad [8]$$

where p is the pressure, ρ is the density and g is the acceleration due to gravity. It is noted that no rotation was imparted to the light phase and it is assumed that there was no frictional interaction between the phases.

Subtract [8] from [7] and eliminate velocities using [1], [2] and [6]; rearrangement gives

$$\frac{F_H'^2}{\sin^2\theta_i} + \frac{X^2 F_H'^2 \tan^2\alpha}{\cos^2\theta_i} - \frac{F_L'^2}{(1 - \sin\theta_i)^2} = X^4 - X^5 \sin\theta_i, \quad [9]$$

where

$$F_H'^2 = \frac{F_H^2}{8\pi^2} = \frac{\rho_H Q_H^2}{8\pi^2 \Delta\rho g h_\infty^5}, \quad [10]$$

$$F_L'^2 = \frac{F_L^2}{8\pi^2} = \frac{\rho_L Q_L^2}{8\pi^2 \Delta\rho g h_\infty^5} \quad [11]$$

and

$$X = \frac{r_i}{h_\infty}, \quad [12]$$

and where $\Delta\rho = (\rho_H - \rho_L)$.

Equation [9] is differentiated with respect to X:

$$2\cos\theta_i \left[\frac{F_H'^2}{\sin^3\theta_i} - \frac{X^2 F_H'^2 \tan^2\alpha \sin\theta_i}{\cos^4\theta_i} + \frac{F_L'^2}{(1 - \sin\theta_i)^3} - \frac{X^5}{2} \right] \frac{d\theta_i}{dX} = \frac{2X F_H'^2 \tan^2\alpha}{\cos^2\theta_i} - 4X^3 + 5X^4 \sin\theta_i. \quad [13]$$

By analogy with the work of Gardner (1988) for two-phase flow into a horizontal offtake, the expression in square brackets set equal to zero is the condition for critical flow, which occurs at the control point. If $d\theta_i/dX$ is to be continuous at the control point, the r.h.s. of [13] must simultaneously equal zero. Therefore, we have the simultaneous equations

$$\frac{F_H'^2}{\sin^3\theta_i} - \frac{X^2F_H'^2\tan^2\alpha\sin\theta_i}{\cos^4\theta_i} + \frac{F_L'^2}{(1-\sin\theta_i)^3} - \frac{X^5}{2} = 0 \qquad [14]$$

and

$$\frac{2F_H'^2\tan^2\alpha}{\cos^2\theta_i} - 4X^2 + 5X^3\sin\theta_i = 0, \qquad [15]$$

which can be solved with the energy equation [9]. F_L is obtained as a function of F_H, where α is a parameter.

When $\alpha = 0^\circ$ we have the solution that $X = 0.8/\sin\theta_i$ and

$$F_H^2 = 0.8^5 2\pi^2 \frac{(2-\sin\theta_i)}{\sin^2\theta_i} \qquad [16]$$

and

$$F_L^2 = 0.8^5 2\pi^2 \frac{(1-\sin\theta_i)^3}{\sin^4\theta_i}, \qquad [17]$$

from which $\sin\theta_i$ can be eliminated algebraically.

Solutions for $\alpha = 0^\circ$, 10°, 30° and 60° are shown in figures 4–7 in terms of $F_L^{0.2}$ vs $F_H^{0.4}$. These powers of the Froude numbers are employed so that linear scales are conveniently used in the graphs but it is also noted that $F_H^{0.4}$ is inversely linearly proportional to h_∞. F_L and F_H can be regarded as dimensionless flow rates, so that figures 4–7 show how the flow rate of one phase affects the flow rate of the other when the liquid level is held constant.

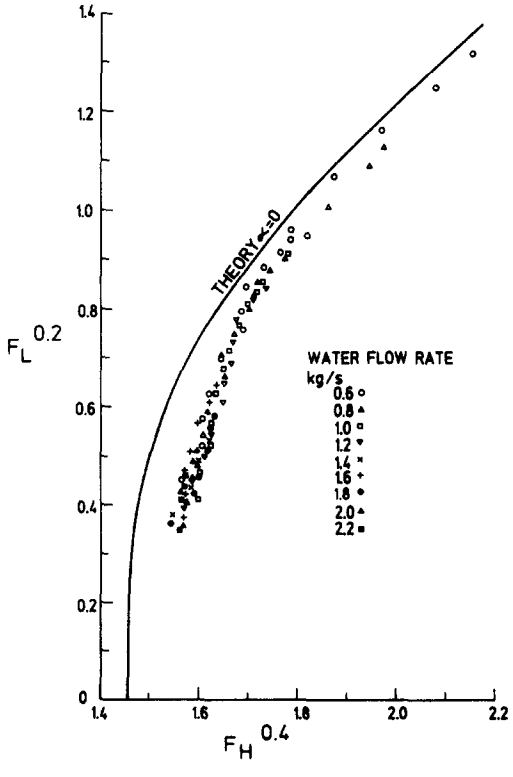

Figure 4. Results for a blade angle of 0 to the radial.

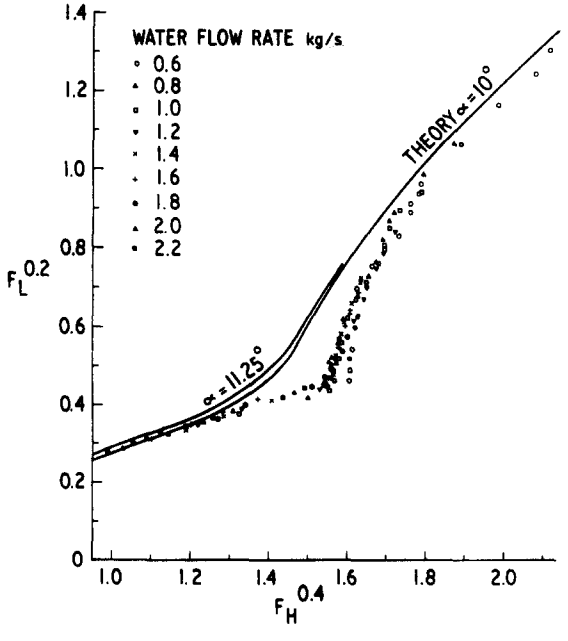

Figure 5. Results for a blade angle of 10° to the radial.

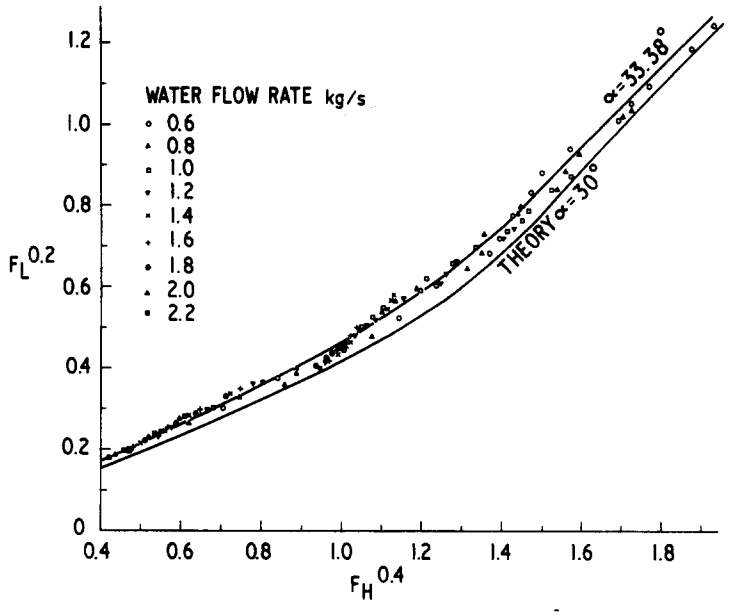

Figure 6. Results for a blade angle of 30° to the radial.

It is also useful to see how the ratio of the volumetric flow rates affects the liquid level. Therefore, figure 8 shows $F_H^{-0.4}$, which can be regarded as a dimensionless level, plotted vs $(F_H/F_L)^{0.4}$, which does not contain the variable h_∞.

The predicted shape of the interface is shown in figures 9(a–d) for $\alpha = 0°$, 10°, 30° and 60° and for three values of $F_H^{0.4}$ for each value of α. The position of the control point is indicated on each shape. If the prediction of F_L as a function of F_H is to be accurate, it is, at least, necessary that the slope of interface at the control point should be radial because of the assumed uniform radial flow in the theory for each point on the interface and because the theory is specifically dependent upon conditions at the control point. It is seen that fair agreement between theory and experiment may be expected in a number of cases. This is especially true when $\alpha = 60°$. The worst case is when $\alpha = 0°$ and $F_H^{0.4} = 1.45$ or $F_H = 2.54$, when the slope of the interface at the control point is far from radial. This corresponds to $F_L = 0$ or the condition for the inception of entrainment without

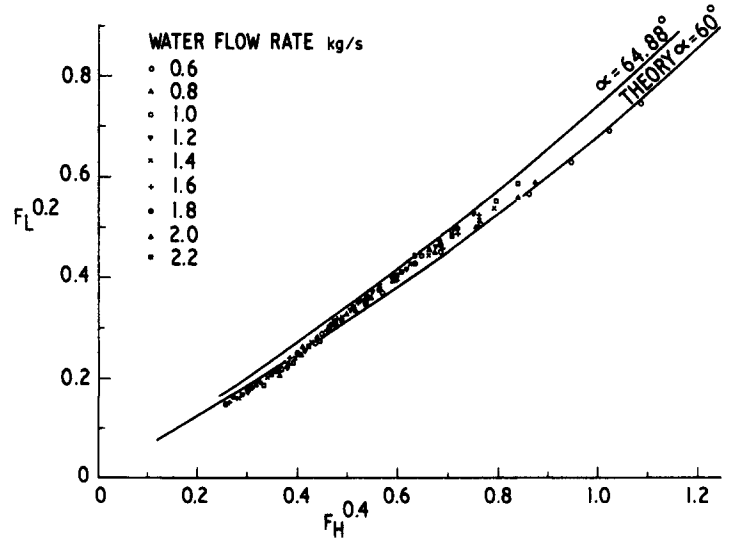

Figure 7. Results for a blade angle of 60° to the radial.

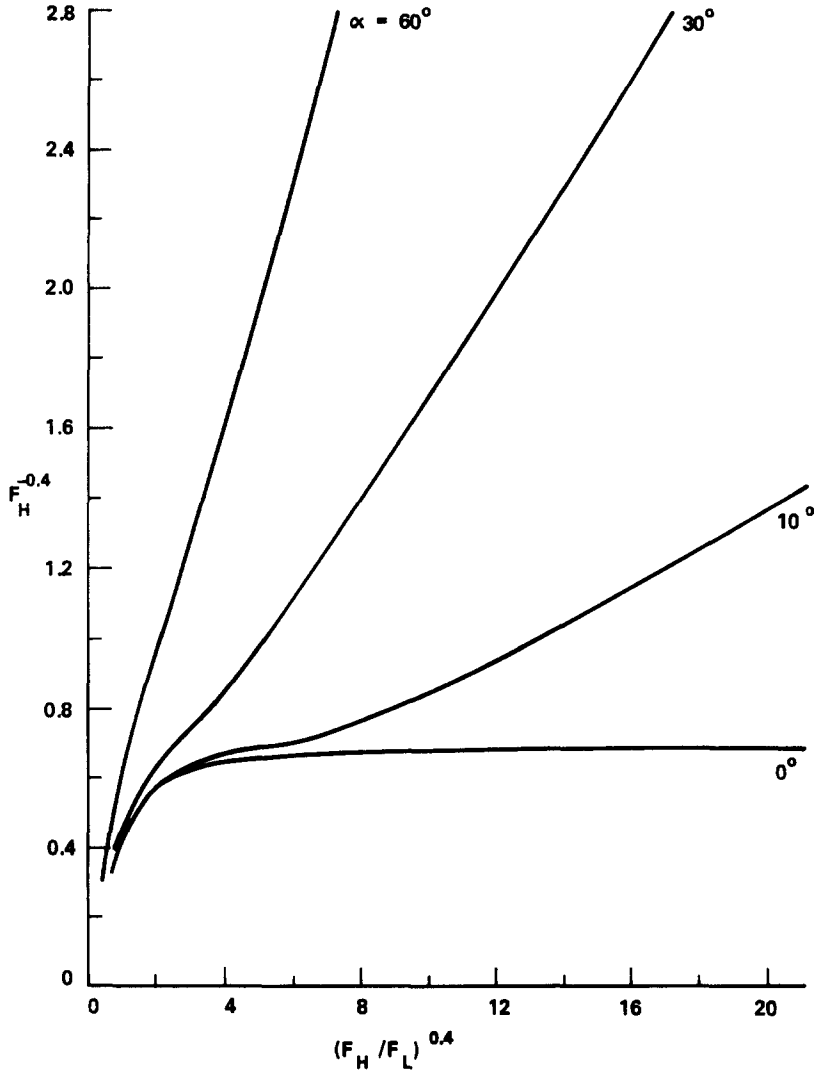

Figure 8. Theoretical values of dimensionless water depth, $F_H^{-0.4}$, vs dimensionless volumetric flow ratio to the power 0.4.

circulation. Therefore, it appears probable, as stated at the beginning of this section, that the assumptions concerning the flow pattern will generally give better agreement between theory and experiment than for the special case of inception of entrainment without circulation.

Before proceeding with a description of the results, it is necessary to discuss an assumption implicit in the use of the apparatus. Because the trailing edge of the blades have a finite thickness of 0.7 mm, the flow discharging from the blades expands and it is a reasonable assumption that the expansion is such that the circulation angle remains unchanged. However, let us assume, as an extreme possibility, that the circulation velocity, v_c, retains the value it has just before issuance from the blades. Detailed calculations will not be given but the result is that the circulation angle remains unchanged for a blade angle of 0° but changes to 11.25°, 33.38° and 64.85° for blade angles of 10°, 30° and 60°, respectively. Theoretical curves for these extreme possibilities are given in figures 5–7.

5. RESULTS

All results obtained with the 14.51 mm diameter outlet are tabulated in the appendix. It is noted that the pressure in the test section increased as either the water or air flow rate increased.

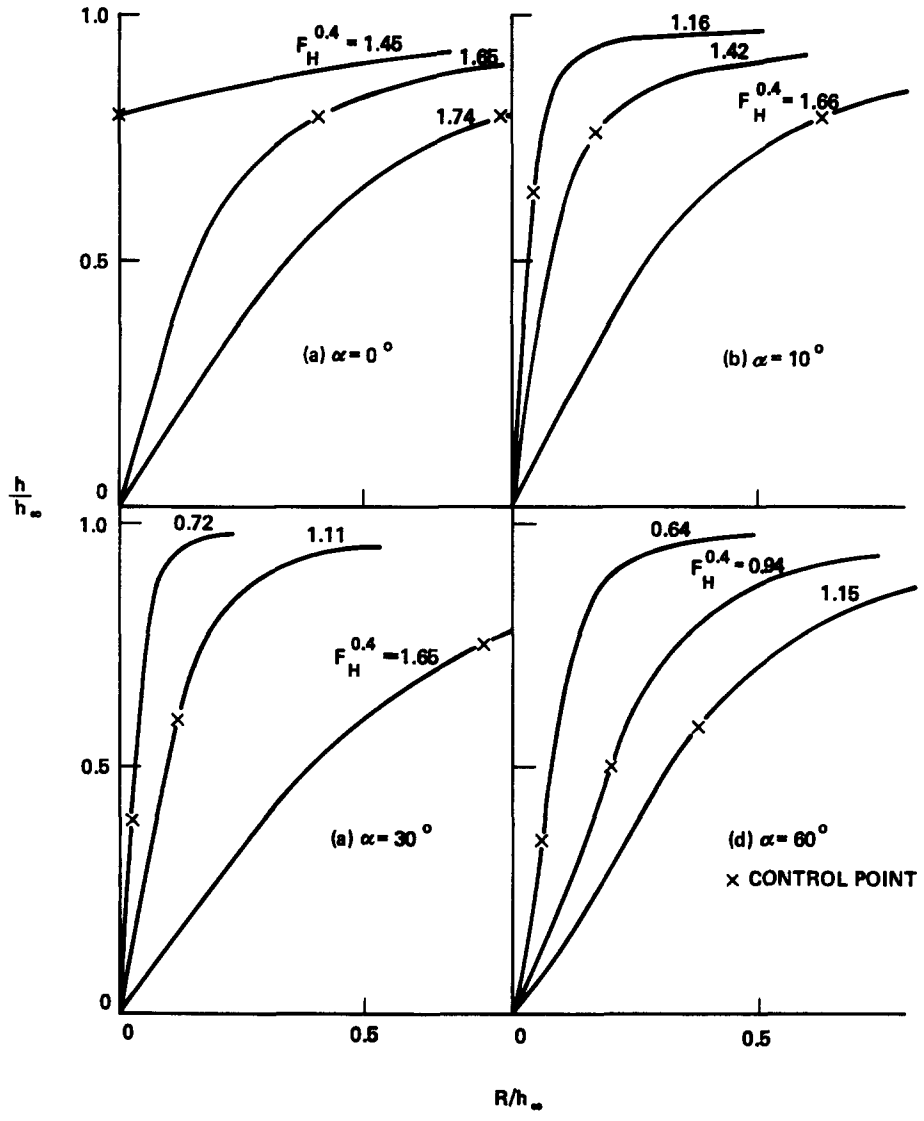

Figure 9. Predicted interface shapes and positions of the control point.

Therefore, because the pressure was limited to about 3 bar, the air flow rate was limited to lower values as the water flow rate increased. However, with blades at 60° to the radial, the water depths were sufficiently large for the larger 26.31 mm outlet to be used to extend the range of results by reducing the operating pressure. Where this outlet is used, it is noted in the appendix.

The water level was measured at a radius of 65 mm from the axis of symmetry and was corrected by an energy balance to estimate h_∞ at an infinite distance from the axis. It was assumed that the water velocity was uniform with respect to the height at the measuring station and that the circulation angle was equal to the blade angle. Both assumptions derive from the assumption that the flow from infinity to the measuring station was potential flow to a line sink at the axis of symmetry. The correction to the water level is (in mm)

$$\Delta h = \frac{305\, W^2}{h_m^2 \cos^2 \alpha},$$

where W(kg/s) is the water flow rate and h_m(mm) is the water depth at the measuring station. The maximum correction was 3.9% and, mostly, was much lower. However, inclusion of the correction significantly improved the correlation of some of the results.

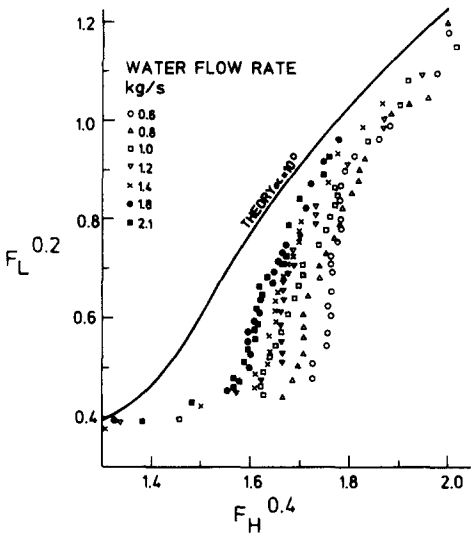

Figure 10. Results with a blade angle of 10° to the radial and with a large 26.31 mm outlet.

Assuming the water to be at 15°C, F_H is readily calculated from the tabulated results. The influence of the air density upon the density difference is negligible compared to the accuracy in measuring, say, h_m. To calculate F_L, the air flow rate at the test vessel's pressure and temperature must be estimated from the rotameter reading in l/min of air at 1 bar and 20°C. This is done by assuming that the pressure drop over the rotameter's bob is independent of the pressure and temperature and is proportional to the gas density times the volumetric flow rate squared. F_L is then calculated using the gas density and the flow rate but it is found that the same result can be obtained by simply substituting the direct rotameter reading for Q_L and the air density at 1 bar and 20°C for ρ_L in the definition of F_L given by [11]. For this reason the accuracy of the measurement of the vessel pressure was not important. The validity of this conclusion was checked by operating a test both with and without the pump in the discharge line operating. This changed the vessel pressure but did not change the measured water level if the flow rate readings of the rotameters were kept the same.

All the tabulated results in terms of F_L and F_H are plotted in figures 4–7 to be compared with the theory. Looking at all the graphs together shows that the use of F_L and F_H alone, as dictated by the theory, provides excellent correlation of the results for each blade angle. That this can be demonstrated is largely due to the care taken by the rig operator, who made measurements without knowing how they would look when plotted. The only points that do not correlate well are a few for a water flow rate of 0.6 kg/s in figure 5. This is probably due to an influence of the offtake diameter. Figure 10 shows some results obtained with a blade angle also at 10° to the radial but with the larger 26.31 mm diameter offtake. It is seen that there is a systematic divergence from a single correlating curve as the water flow rate is changed in the same region as the divergence for a single water flow rate is seen in figure 5. It was chiefly because of this that most of the work was carried out with the smaller outlet.

It is interesting that the divergence is greatest for an intermediate range of flow rates. When F_H is small, the water depth is largest and it is understandable that a good correlation is obtained. When F_H is large, although the water depth becomes small, figure 9(b) shows that the control point moves away from the outlet and this explains why a fair correlation is obtained in that region. It is also support for the ideas embodied in the theory.

Figure 4 for water flow without circulation shows fairly close agreement with the theory for larger values of F_L but the agreement for $F_L^{0.2} < \sim 0.7$ is not so good. Extrapolation of the results to $F_L = 0$ gives the condition for the inception of entrainment to be $F_H^{0.4} = 1.54$ to compare with a theoretical value of 1.45. This represents an error in the theoretical value of the water level of 6.2%.

Experimental results for blades at 10° to the radial in figure 5 show a sharp break at $F_L^{0.2} = 0.45$. For higher values of $F_L^{0.2}$ they follow the trend for radial blades and indeed, have almost the same

numerical values. For lower values of $F_L^{0.2}$, $F_L^{0.2}$ varies much more slowly with $F_H^{0.4}$. The theoretical curve irons out the sudden change but, otherwise tends to fair agreement with the experimental results for high and low air flow rates. The intermediate region, where not such good agreement is found, can be appreciated qualitatively from the positions of the control points on the theoretical interface shapes given in figure 9(b).

The results with the blade angle at 30° to the radial are given in figure 6 and show fair agreement with theory. This would be expected from the positions of the control points on the predicted interface shapes in figure 9(c). Agreement is rather better with the theoretical curve for the equivalent blade angle of 33.38° obtained from the extreme assumptions regarding discharge of water from the blades given in the last section. However, this does not allow one to conclude that the experimental results are a set with the circulation angle far from the axis of symmetry equal to 33.38°.

There is fine detail in the trends of the results shown in figure 6. In particular, the onset of circulation of the vortex is seen at a break in the trend at $F_L^{0.2} = 0.4$ and $F_H^{0.4} = 0.95$. The rotation of the vortex stopped at about $F_H^{0.4} = 1.25$ but this is not so evident in figure 6. It is seen that data with a rotating vortex correlated without any evidence for the need for an extra correlating parameter. More surprising is that rotation did not cause greater divergence from the theoretical curve.

Figure 7 gives results for a blade angle at 60° to the radial and it is remembered that some results using the larger outlet are included. Agreement with the theoretical curve is excellent, though close examination shows differences in slope which make the experimental results appear to wind themselves around the theoretical curve. The results agree rather less well with the theoretical curve for an equivalent blade angle of 64.85° obtained using extreme assumptions regarding discharge of water from the blades.

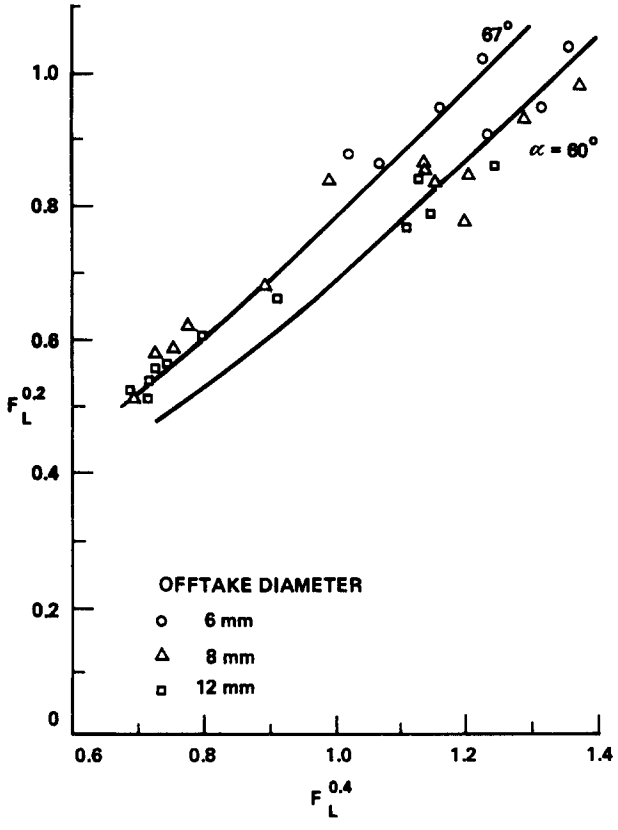

Figure 11. Results of Smoglie & Reimann (1986) for a bottom offtake compared with theory.

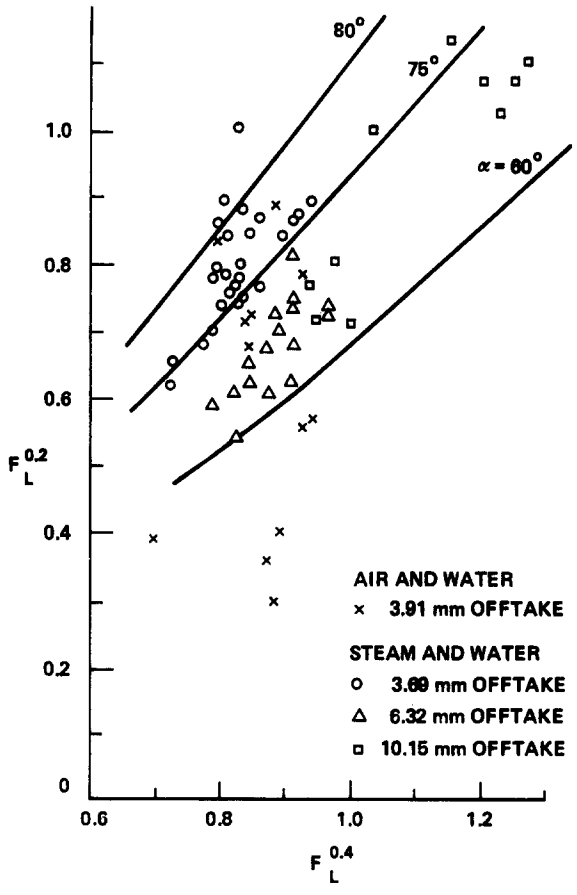

Figure 12. Results of Schrock *et al.* (1986) for a bottom offtake compared with theory.

6. COMPARISON WITH OTHER EXPERIMENTAL WORK

Smoglie & Reimann (1986) carried out investigations in which water and air flowed slowly and cocurrently in a 206 mm bore pipe at pressures between 2.3 and 5.4 bar. A mixture was either drawn from the top or bottom of the pipe and, insofar as the present theory may apply, the rôles of the heavy and light phases in the theory would be reversed when drawing from the top of the pipe. Experimental results were tabulated in Smoglie's (1984) thesis.

Schrock *et al.* (1986) carried out similar experiments in a 102.3 mm diameter tube with air and water at pressures between 2.7 and 6.7 bar and with steam and water at pressures between 2.6 and 9.8 bar. They tabulated their results.

There are, at least, two reasons why these results are not directly comparable with the present work. First, neither set of authors measured the circulation in either phase and it could have been occurring in either or both. Second, there was crossflow over the discharge, even though it was weak. That the direction of flow can be important is illustrated by some tests carried out by the present author in an 84 mm horizontal tube. The tube was filled with water and suction was applied to a tube set in the top of the circumference. Air was allowed to be drawn into the 84 mm tube either from one or both ends and, for a given suction, the final state was a stationary pool of water which had the depth required for incipient entrainment by the air flow. The value of $F_L^{0.4}$ for this incipient entrainment varied with air flow rate from 0.98 to 1.07, when air was drawn in from one end of the horizontal tube, and from 1.28 to 1.41 when air was drawn in from both ends.

Notwithstanding the differences just described, it seems worthwhile examining the data from the two sets of authors above to see what value of the circulation angle α might account for the results if everything else was equal.

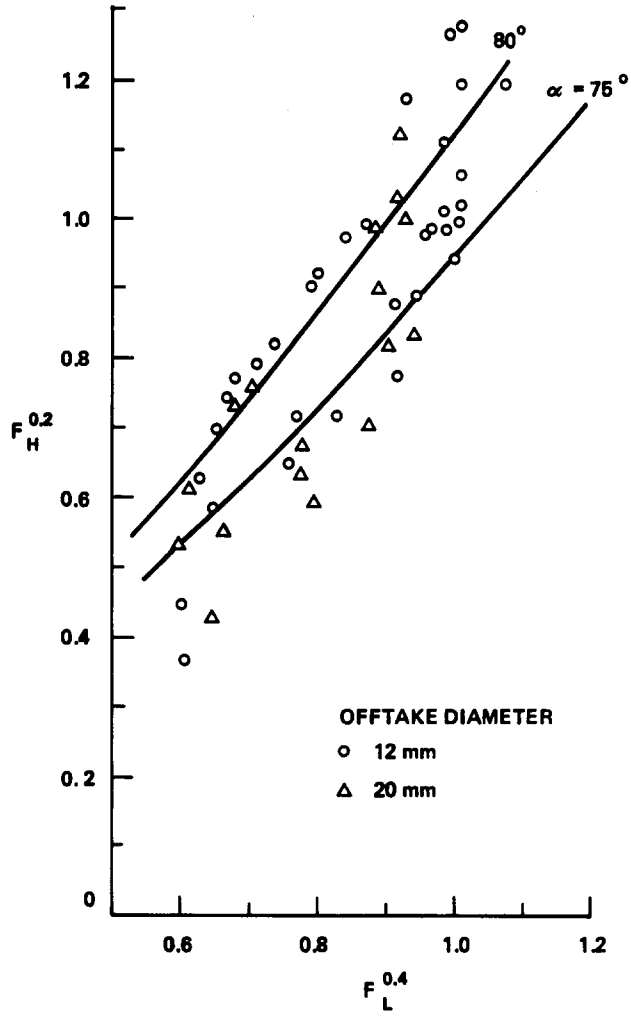

Figure 13. Results of Smoglie & Reimann (1986) for a top offtake compared with theory.

Figures 11–14 show the results of Smoglie & Reimann (1986) and Shrock *et al.* (1986) for extraction through both bottom (figures 11 and 12) and top (figures 13 and 14) offtakes. Sample curves from the theory are given in each figure on the assumption that circulation only occurs in the water phase for bottom offtakes and in the air or steam phase for top offtakes.

The evidence from figures 11–14 is confusing and the reader is left to draw his own conclusions. Nevertheless, the following observations are recorded. Data points often approximately follow the trends indicated by the theoretical lines and, then, the effective circulation angle does not vary greatly with changes in the flow rate. However, this statement is not true for the air–water data in figure 12. Figures 11 and 13 from the same source indicate that the diameter of the offtake has no influence on the results. Figure 12 indicates that changing the offtake diameter from 6.32 to 10.15 mm does not affect the results. Alternatively, the results in this figure for offtakes of 3.69, 3.91 and 6.32 mm agree with each other and lie in a vertical band crossing the theoretical curves. However, this is contradicted by the results shown in figure 14 for a top offtake of 3.76 mm as opposed to the results in figure 12 from the same source for a bottom offtake. The results in figure 14 approximately follow the trends of the theoretical lines.

Overall it is seen that an effective circulation angle is usually greater than 45° and an argument which predicts an angle of such a magnitude can be constructed as follows. Consider a bottom offtake where the heavy phase flows towards the offtake with a velocity $v = Q_H/A$, where A is the flow area, which, on the assumption that h_∞/D is small, is approx. $4D^{1/2}h_\infty^{3/2}/3$. D is the diameter

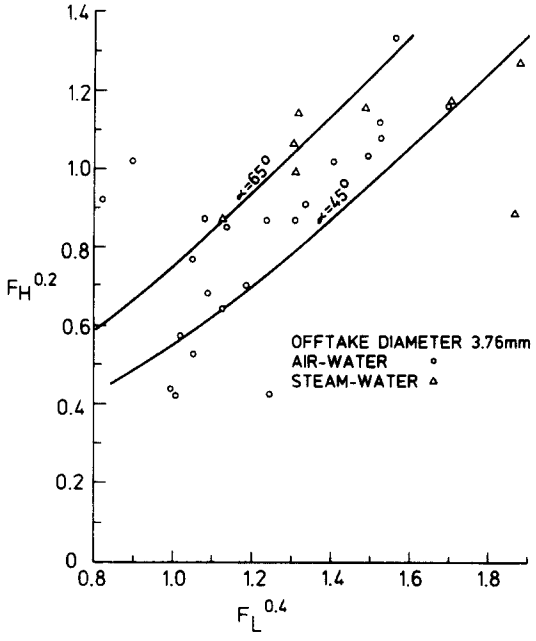

Figure 14. Results of Schrock *et al.* (1986) for a top offtake compared with theory.

of the horizontal tube. Assume that a vortex forms around the offtake with a diameter equal to the width, w, of the interface in the horizontal tube and, further, assume that the velocity at the radius $w/2$ is v. It is noted that $w \simeq 2D^{1/2}h_\infty^{1/2}$. Now the velocity vector is at an angle α to the radial and, therefore, the circulation velocity is $v \sin\alpha$ and the circulation is $C = vw \sin\alpha/2 = 3Q_H \sin\alpha/4h_\infty$. The circulation constant is also defined by [3] and [6] and, thus, $\cos\alpha = 2/3\pi$ or $\alpha = 78°$. If the radius at which the velocity in the vortex equalled v was $w/4$, then $\cos\alpha = 4/3\pi$ or $\alpha = 65°$.

7. CONCLUSIONS

An ideal system has been studied experimentally in which a uniform flow of water with a given circulation approaches an offtake of small dimensions in the flat bottom of a vessel and entrains supernatant air.

Results for any given circulation angle are correlated by two dimensionless groups involving the flow rates of the two phases, the densities of the two phases, acceleration due to gravity and the depth of flow far from the offtake. The diameter of the offtake is not a variable, as long as it is sufficiently small.

An approximate theory agrees with the results satisfactorily for most purposes and the agreement improves as the circulation angle increases. The agreement is good for circulation angles of 30° and 60° and the depth of flow is predicted within 6.2% with radial flow or a circulation angle of 0°.

The study provides a useful background for understanding the discharge of steam and water from small breaks in certain PWR LOCAs. Other workers have studied this problem in a geometrical configuration closely resembling that in the PWR. Their results are compared graphically with theoretical curves for constant circulation angles.

Acknowledgements—Mr J. Barker manufactured the test vessels and Mr P. L. Hanks painstakingly conducted the experiments. Both are thanked.

This work was carried out at the National Power Technology and Environmental Centre and is published by permission of the Central Electricity Generating Board.

Editors' note—The Editors wish Dr G. C. Gardner well in his retirement. Over the years he has contributed to the journal and assisted us in many ways, for which we are grateful.

REFERENCES

ANDERSON, J. L. & BENEDETTI, R. L. 1986 Critical flow through small pipe breaks. EPRI Report No. NP-4532.

BINNIE, A. M. & TEARE, J. D. 1956 Experiments on the flow of swirling water through a pressure nozzle and an open trumpet. *Proc. R. Soc.* **235A,** 78–89.

DAVIDIAN, J. & GLOVER, J. E. 1956 Development of a non-circulatory water spout. *Trans. ASCE* **HY4,** Paper 1038-3.

GARDNER, G. C. 1988 Co-current flow of air and water from a reservoir into a short horizontal pipe. *Int. J. Multiphase Flow* **14,** 375–388.

GARDNER, G. C. & CROW, I. G. 1971 Onset of drawdown of supernatant fluids in surge tanks. *Chem. Engng Sci.* **26,** 211–219.

GULLIVER, J. S. & RINDELS, A. J. 1987 Weak vortices at vertical intakes. *Trans. ASCE J. hydraul. Div.* **113,** 1101–1116.

HARLEMAN, D. R., MORGAN, R. L. & PURPLE, R. A. 1959 Selective withdrawal from a vertically stratified fluid. Presented at the *Int. Association for Hydraulic Research, 8th Congress*, Paper No. 10-C.

JAIN, A. K., KITTUR, G., RAJU, R. & GARDE, R. J. 1978 Air entrainment in radial flow towards intakes. *Trans. ASCE J. hydraul. Div.* **104,** 1323–1329.

JAIN, S. C. 1987 Free swirling flows in a vertical dropshaft. *Trans. ASCE J. hydraul. Div.* **113,** 1277–1289.

LUBIN, B. T. & SPRINGER, G. S. 1967 The formation of a dip on the surface of a liquid draining from a tank. *J. Fluid Mech.* **29,** 385–390.

MUNSON, B. R. 1988 The effect of a moving sink on selective withdrawal from a discretely stratified fluid. *Phys. Fluids* **31,** 2720–2722.

SCHROCK, V. E., REVANKAR, S. T., MANNHEIMER, R. & WANG, C-H. 1986 Small break critical discharge—the roles of vapour and liquid entrainment in stratified region upstream of break. Report NUREG/CR-4761.

SMOGLIE, C. 1984 Two-phase flow through small branches in a horizontal pipe with stratified flow. Report KfK 3861, Translation of a Dissertation, Faculty of Mech. Engng, Univ. Karlsruhe, F.R.G.

SMOGLIE, C. & REIMANN, J. 1986 Two-phase flow through small branches in a horizontal pipe with stratified flow. *Int. J. Multiphase Flow* **12,** 609-625.

SPRINGER, E. K. & PATTERSON, F. M. 1969 Experimental investigation of critical submergence for vortexing in a vertical cylindrical tank. *Am. Soc. mech. Engrs*, Paper No. 69-FE-49.

APPENDIX

Tables of Results

The notation used in the following tables is:

A—air flow rate at 1 bar and 20°C—the direct rotameter reading (l/min).
h_m—the measured depth 65 mm from the axis of symmetry (mmH_2O).
P—the vessel pressure above atmospheric (mmHg).

All results were obtained using a 14.51 mm bore offtake, except those marked † where a 26.31 mm offtake was used.

Table A1. Results for a blade angle of 0° to the radial

A (l/min)	h_m (mmH_2O)	P (mmHg)	A (l/min)	h_m (mmH_2O)	P (mmHg)
	$W = 0.6 kg/s$			$W = 1.2 kg/s$	
6.5	20.5	88	6.5	26.8	343
12	20.0	122	12	26.4	397
20	20.0	155	20	26.0	481
30	19.8	193	30	25.8	596
50	19.5	228	50	25.4	752
70	19.0	274	70	25.3	864
90	19.0	325	90	25.1	978
120	18.9	392	120	25.0	1102
140	18.5	447	160	24.9	1345
160	18.1	482	200	24.4	1474
180	17.9	506	220	24.0	1573
200	17.9	539		$W = 1.4 kg/s$	
300	17.0	725	6.5	28.8	453
400	16.1	941	12	28.1	536
500	15.2	1231	20	27.9	633
600	14.6	1474	30	27.4	759
	$W = 0.8 kg/s$			$W = 1.6 kg/s$	
6.5	23.0	158	6.5	29.9	578
12	22.5	201	12	29.8	688
20	22.3	244	20	29.8	821
30	22.2	293	30	29.6	942
50	21.7	360	50	29.2	1198
70	21.8	428	70	28.8	1387
90	21.4	498	90	28.5	1604
120	21.0	582		$W = 1.8 kg/s$	
140	20.9	629	6.5	31.8	763
160	20.8	670	12	30.7	859
180	20.5	718	20	30.5	991
200	20.1	790	30	30.2	1182
300	19.1	1071	50	30.0	1472
400	18.2	1423	60	29.9	1656
457	17.9	1811		$W = 2.0 kg/s$	
	$W = 1.0 kg/s$		6.5	32.5	905
6.5	24.5	240	12	32.3	1035
12	24.4	285	20	32.1	1257
20	24.1	348	30	31.9	1438
30	24.1	429	38	31.8	1604
50	23.9	542		$W = 2.2 kg/s$	
70	23.7	625	6.5	33.8	1097
90	23.5	713	12	33.7	1242
120	23.2	818	20	33.5	1449
160	22.9	948	24	33.5	1542
180	22.7	1030			
200	22.5	1097			
250	21.9	1304			
300	21.3	1656			

Table A2. Results for a blade angle of 10° to the radial

A (l/min)	h_m (mmH_2O)	P (mmHg)	A (l/min)	h_m (mmH_2O)	P (mmHg)
	$W = 0.6 kg/s$			$W = 1.4 kg/s$	
6.5	20.0	88	6.5	38.1	421
9	20.0	116	9	35.0	456
12	20.0	132	12	31.9	494
15	19.9	150	15	29.0	529
20	19.8	170	20	28.5	605
30	19.8	199	30	28.4	741
50	19.8	238	50	28.1	921
70	19.3	290	70	27.9	1055
90	18.9	338	90	27.6	1216
120	18.5	409	110	27.4	1340
140	18.2	444	130	27.2	1469
160	18.2	481	140	27.1	1547
180	18.0	513		$W = 1.6 kg/s$	
200	17.9	542	6.5	43.5	572
300	16.9	596	9	39.8	599
400	16.0	854	12	37.0	647
500	15.2	1138	15	34.5	705
600	14.9	1438	20	30.3	765
	$W = 0.8 kg/s$		30	30.0	923
6.5	24.0	139	50	29.6	1154
9	23.3	159	70	29.3	1449
15	22.9	201	90	29.1	1557
24	22.8	257		$W = 1.8 kg/s$	
40	22.6	318	6.5	47.5	692
60	22.1	390	9	44.7	766
80	21.7	450	12	39.5	817
100	21.1	513	15	37.0	860
140	21.4	605	20	32.5	941
180	21.0	691	24	31.7	967
200	20.8	743	30	31.4	1107
300	19.9	958	45	30.9	1345
400	19.0	1392	60	30.5	1541
	$W = 1.0 kg/s$			$W = 2.0 kg/s$	
6.5	29.8	212	6.5	51.0	847
9	25.2	240	9	45.5	973
12	25.0	268	12	42.0	967
20	24.8	337	15	39.5	967
30	24.7	418	20	35.0	1149
50	24.5	514	24	33.0	1231
70	24.1	586	40	32.7	1474
90	23.7	664	44	32.0	1656
120	23.2	757		$W = 2.2 kg/s$	
160	23.0	907	6.5	55.0	1019
200	22.8	967	9	49.2	1097
250	22.5	1231	12	45.0	1097
300	21.7	1500	15	42.0	1221
	$W = 1.2 kg/s$		20	37.0	1361
6.5	34.9	309	24	35.5	1464
9	31.9	327	30	33.8	1474
12	27.5	373			
15	27.0	409			
24	26.8	503			
40	26.6	632			
60	25.9	774			
80	25.5	880			
100	25.4	957			
140	24.9	1154			
180	24.6	1361			
224	24.3	1604			

Table A3. Results for a blade angle of 30° to the radial

A (l/min)	h_m (mmH_2O)	P (mmHg)	A (l/min)	h_m (mmH_2O)	P (mmHg)
	W = 0.6 kg/s			*W = 1.2 kg/s*	
6.5	46.3	83	6.5	79.4	332
12	38.8	114	9	74.6	361
20	32.5	147	15	64.1	436
30	28.4	177	24	55.0	529
50	26.2	215	30	44.6	583
70	23.6	269	40	42.8	676
90	23.2	311	50	41.2	759
120	22.6	346	60	40.2	833
160	21.9	436	70	39.3	901
200	21.5	506	90	36.8	996
250	20.5	617	100	34.0	1146
300	19.0	682	120	33.6	1242
350	18.6	810	140	33.2	1350
400	18.1	889	173	30.0	1449
500	17.0	1071	193	29.4	1562
600	16.5	1459			
	W = 0.8 kg/s			*W = 1.4 kg/s*	
6.5	59.0	149	6.5	91.3	448
12	48.8	189	9	82.2	479
20	41.1	237	15	73.8	561
30	33.8	299	24	62.9	690
50	33.0	374	30	48.0	777
60	32.0	404	40	45.8	875
70	30.5	421	50	44.3	977
80	27.5	440	70	43.0	1154
100	26.7	551	90	41.0	1288
140	26.6	659	110	40.2	1459
160	25.1	753	123	40.4	1537
180	24.8	819		*W = 1.6 kg/s*	
200	23.3	824	6.5	100.0	610
250	23.0	944	12	84.7	691
300	22.4	1086	20	74.4	806
400	21.0	1443	30	64.1	967
425	20.6	1542	40	49.8	1102
			50	48.4	1211
	W = 1.0 kg/s		70	46.4	1449
6.5	72.5	227	82	45.8	1547
12	58.9	282		*W = 1.8 kg/s*	
20	49.5	347	6.5	107.0	756
30	39.5	419	9	99.2	793
50	37.8	533	15	86.8	905
60	36.8	600	20	80.0	973
70	36.0	644	30	70.8	1187
80	33.0	674	40	53.5	1304
100	32.6	770	50	52.0	1459
120	31.0	844	60	50.1	1593
140	29.5	993		*W = 2.0 kg/s*	
160	27.8	1030	6.5	121.0	885
180	27.0	1097	12	101.5	1004
200	26.7	1159	20	88.0	1200
250	25.6	1330	30	61.0	1350
285	24.8	1553	40	59.0	1562
				W = 2.2 kg/s	
			6.5	130.2	1081
			9	117.0	1128
			15	99.7	1299
			24	89.0	1495

Table A4. Results for a blade angle of 60° to the radial

A (l/min)	h_m (mmH_2O)	P (mmHg)	A (l/min)	h_m (mmH_2O)	P (mmHg)
	W = 0.6 kg/s			*W = 1.6 kg/s*	
6.5	88.0	89	6.5	183.5	581
12	74.6	116	12	148.0	680
20	66.0	143	24	125.5	867
30	57.0	170	40	107.5	1107
50	47.2	218	60	99.2	1324
70	42.4	260	80	90.8	1547
90	37.5	319	100†	81.0	228
120	34.1	351	140†	70.0	287
160	31.5	432	180†	66.4	327
200	29.5	543	220†	62.7	360
	W = 0.8 kg/s			*W = 1.8 kg/s*	
6.5	100.8	152	6.5	196.3	720
12	89.7	189	12	164.0	859
20	82.9	240	20	140.5	973
30	73.5	291	30	126.5	1154
50	61.9	374	50	113.0	1469
70	54.1	544	70†	97.5	234
90	48.0	530	90†	91.2	274
120	43.0	636	120†	82.0	310
160	40.8	726	160†	75.9	361
180	39.0	848	200†	72.0	403
	W = 1.0 kg/s		220†	70.3	426
6.5	120.1	224		*W = 2.0 kg/s*	
12	102.5	285	10	191.5	965
20	91.2	347	15	165.5	1086
30	86.2	417	24	144.0	1278
50	74.2	557	40	128.4	1583
70	66.4	662	60†	110.0	273
90	61.3	759	80†	102.0	307
120	56.0	918	100†	96.7	337
140	49.8	978	140†	89.0	388
192	47.0	1252	180†	80.0	457
	W = 1.2 kg/s		220†	76.5	502
6.5	143.0	322		*W = 2.2 kg/s*	
12	115.8	399	10	195.0	1190
20	103.7	481	15	179.5	1299
30	96.8	586	24	156.8	1500
50	85.0	762	40†	133.0	278
70	78.0	896	70†	115.5	336
90	69.4	1041	90†	107.0	365
120	63.3	1219	120†	100.6	416
160	58.0	1443	160†	90.7	488
180	56.8	1555	200†	85.7	546
	W = 1.4 kg/s		243†	76.5	642
6.5	162.0	428			
12	135.1	511			
20	116.5	608			
30	104.0	782			
50	93.4	988			
70	85.2	1159			
90	81.0	1330			
118	73.0	1568			
140†	65.0	230			
180†	59.8	259			
200†	57.0	261			